Wavelet-Based Optical Flow Estimation

Li-Fen Chen, *Member, IEEE*, Hong-Yuan Mark Liao, *Senior Member, IEEE*, and Ja-Chen Lin

***Abstract*—In this paper, a new algorithm for accurate optical flow (OF) estimation using discrete wavelet approximation is proposed. The computation of OF depends on minimizing the image and smoothness constraints. The proposed method takes advantages of the nature of wavelet theory, which can efficiently and accurately approximate any function. OF vectors and image functions are represented by means of linear combinations of scaling basis functions. Based on such wavelet-based approximation, the leading coefficients of these basis functions carry global information about the approximated functions. The proposed method can successfully convert the problem of minimizing a constraint function into that of solving a linear system of a quadratic and convex function of scaling coefficients. Once all the corresponding coefficients are determined, the flow vectors can be obtained accordingly. Experiments have been conducted on both synthetic and real image sequences. In terms of accuracy, the results show that our approach outperforms the existing methods which adopted the same objective function as ours.**

***Index Terms*—Optical flow estimation, scaling basis function, wavelets.**

I. Introduction

OPTICAL flow (OF) estimation is an essential problem in motion analysis of image sequences. It provides information needed for video technology, such as object tracking, image segmentation, and motion compensation. A great number of approaches for OF estimation have been proposed in the literature, including gradient-based, correlation-based, energy-based, and phase-based techniques [1]–[3]. A typical gradient-based approach was proposed by Horn and Schunck [4], which is mainly based on optimizing an energy function E that is a function of an image constraint and a smoothness constraint

$$E = \int\int [(I_x u + I_y v + I_t)^2 + \alpha(|\nabla u|^2 + |\nabla v|^2)]\, dx\, dy \quad (1)$$

where

I	$= I(x, y; t)$—image brightness function at time t;
$[u, v]$	$= [u(x, y), v(x, y)]$—the flow vector;
∇	gradient operator;
I_x, I_y, I_t	partial derivatives of $I(x, y; t)$ with respect to the x- and y- coordinate, and time t, respectively.

The first term on the right-hand side of (1) is the image constraint, the second term is the smoothness constraint, and α is the weighting between the two constraints. The image constraint is derived from the first-order Taylor expansion of the brightness constancy assumption $I(x + u\delta t, y + v\delta t; t + \delta t) = I(x, y; t)$. For each pixel (x, y), two variables, u and v, need to be solved. With only one constraint (the image constraint), the solution of u and v cannot be obtained. Thus, Horn and Schunck proposed the smoothness constraint and added it into the objective function shown in (1). Under these circumstances, the flow field can be solved by optimizing the objective function. It is known that the smoothness constraint may be invalid across the motion boundary, but this problem can be solved by using the regularization technique [5].

Another major concern is the approximation errors that occur when the gradient-based approach is adopted. These errors are due to inaccurate numerical approximation of partial derivatives, as well as temporal and spatial aliasing during sampling of the image brightness function $I(x, y; t)$. In order to solve the above-mentioned error problem, Barron *et al.* [1] proposed an improved approach based on (1). They suggested applying a spatiotemporal pre-smoothing to the target image first. Then, a four-point central difference technique is adopted to simulate the differentiation operation. Their method significantly improved the method proposed by Horn and Schunck [4] because the smoothing step is added. In [2], Lai and Vemuri pointed out the approximation error problem and concluded that in the image constraint, large approximation errors are usually located in areas with large nonlinear components or in those with fast temporal or spatial changes in the brightness function. Therefore, they proposed a reliability testing scheme to determine whether each pixel in the image is adequate for the image constraint or not.

In general, there are two possible ways to solve the optimization problem for the energy function shown in (1). The first is to convert the optimization problem into one of solving partial differential equations based on variational calculus [1], [4]. This kind of approach estimates flow vectors iteratively. The other kind of approach directly uses the discrete version of (1) to calculate the flow vectors [6], [2]. The discretization process converts the original optimization problem into the problem of solving a linear system. However, such intuitive discretization might lose precision of the original energy function and information about the interaction between the image brightness function and the flow field. In this paper, we will introduce the concept of wavelets to solve the optical-flow estimation problem.

The wavelet is a mathematical tool used to describe functions more efficiently and precisely. It has been shown to be a useful tool and is widely used in various applications [7]–[10].

Manuscript received November 17, 2000; revised October 30, 2001. This paper was recommended by Associate Editor J.-N. Hwang.

L.-F. Chen is with the Integrated Brain Research Unit, Department of Medical Research and Education, Taipei Veteran's General Hospital, Taipei 112, Taiwan R.O.C. (e-mail: lfchen3@vghtpe.gov.tw).

H.-Y. M. Liao is with the Institute of Information Science 20, Academia Sinica, Taipei 115, Taiwan R.O.C. (e-mail: liao@iis.sinica.edu.tw).

J.-C. Lin is with the Department of Computer and Information Science, National Chiao Tung University, Hsinchu 300, Taiwan (e-mail: jclin@cis.nctu.edu.tw).

Publisher Item Identifier S 1051-8215(02)01124-2.

Some wavelet-based OF estimation approaches have been proposed [11]–[15]. In [11], Burns *et al.* proposed a 3-D transform to the flow field and required large sequences of consecutive pictures for flow estimation. It is a quite different methodology than ours, since we only have to use two consecutive images to estimate flow field. In [12], Bernard assumed that the OF was locally constant. Therefore, an inner product could be made between an image and a set of selected scaling bases such that a linear system which contained all the flow vectors could be generated. In his approach, every flow vector is calculated independently since the smoothness constraint is not considered. Similarly, Srinivasan and Chellappa [13] proposed a similar approach which modeled the OF field using a set of overlapping basis functions. After their model is applied, the image constraint function can be reduced to a scaler equation by integrating with a suitably chosen kernel. The difference between the work proposed in [12] and that in [13] lies in the selection of the basis function for modeling the flow field and some related function variables. Wu *et al.* [14], [15] used wavelets to model flow vectors and proposed a coarse-to-fine hierarchy to reconstruct these vectors. At each iteration, they estimate the wavelet coefficients by minimizing the sum of the squared intensity difference between the warped image and the second image. Basically, the main difference between our work and Wu *et al.*'s [15] is the objective function used for flow field computation. The first-order Taylor expansion we used is known as a kind of approximation of the brightness constancy assumption. The advantage of such approximation is to increase the efficiency of computation, while the disadvantage is to compromise the accuracy. Nevertheless, the key idea in this paper is to present a basic methodology for solving elliptic partial differential systems efficiently and accurately. Meanwhile, Wu *et al.* [14], [15] only applied wavelets to represent u and v. That is, they only used wavelets to approximate the function variable part.

In this paper, the scaling functions are used to approximate both the flow vectors and the image related operators, such as the differentiation operator. Using wavelet calculus, we can efficiently compute derivatives of the functions in terms of the scaling expansion coefficients. After we apply our wavelet model, the energy constraint function of the flow vector becomes a quadratic and convex function of the scaling coefficients. Therefore, we can successfully convert the problem of minimizing a constraint function into that of solving a linear system of a quadratic and convex function of the scaling coefficients. Such conversion preserves the interaction information between flow field and the image related functions, and estimates flow vectors as global minima. Once all the the scaling coefficients are obtained, the flow vectors to be solved can be determined. At the end of this paper, we will discuss experiments conducted on a set of standard test image sequences, including synthetic and real image sequences. The results for standard sequences show that our approach outperforms the existing methods in terms of accuracy. The rest of the paper is organized as follows. In Section II, some key concepts of wavelet theory will be introduced. Then, the proposed solution of the OF problem will be clearly described in Section III. Experimental results will be given in Section IV. Finally, concluding remarks will be made in Section VI.

II. Wavelet Theory

Since wavelet approximation will be applied to derive the solution of the OF problem, in what follows, we will introduce some key concepts of wavelet theory. Basically, the process of wavelet approximation is that of representing a continuous function $f(x)$ with a limited number of successive approximations, each of which is basically a smoothed version of $f(x)$ [16]. Denote the scaling function by $\phi(x)$ and its dilation and translation functions $2^{j/2}\phi(2^j x - n)$ by $\phi_{j,n}(x)$ for $j, n \in Z$, where Z denotes the set of integers. Let V_j be the subspace spanned by $\phi_{j,n}(x)_{n\in Z}$, where $\phi_{j,n}(x)_{n\in Z}$ is an orthonormal basis of V_j. The function spaces $V_j, j \in Z$ have the following properties [16]:

1) $V_j \subseteq V_{j-1}, \quad$ for all $j \in Z$

2) $\bigcup_{j=-\infty}^{\infty} V_j = L^2(R) \quad$ and $\quad \bigcap_{j=-\infty}^{\infty} V_j = \{0\}$

3) a scaling function $\phi(x) \in V_0$ exists such that the set $\{\phi(x-n)\}_{n\in Z}$ is an orthonormal basis of V_0.

Here, R denotes the set of real numbers and $L^2(R)$ denotes the vector space of measurable, square-integrable functions $f(x)$, respectively. Since $\{\phi(x-n)\}_{n\in Z}$ is a basis of V_0, for a function $f(x) \in V_0$, we have

$$f(x) = \sum_n c_n \phi(x-n) \tag{2}$$

where $\{c_n\}_{n\in Z}$ is a sequence and $c_n = \int f(x)\phi(x-n)\,dx$ represents the weighting coefficients for $f(x)$ [17]. In the computation of OF, we will represent the flow vector and image related functions based on (2). More precisely, we will not make use of the multiresolution concept of wavelets in this paper. In addition, the Daubechies scaling function [18] will be used as the basis of V_0 since the Daubechies scaling functions have the properties of compact support and orthogonality. In what follows, we will describe the relation between the wavelet transform and differential operators, which has been well treated in [7].

First, we represent the function $f(x) = \sum_n c_n\phi(x-n)$ as defined in (2), where $c_n = \int f(x)\phi(x-n)\,dx$. Since $\int \phi(x-n)\,dx = 1$ and $\phi(x)$ is compactly supported, we can think of $\phi(x-n)$ as a function which is similar to a delta function. Therefore, we have

$$f(n) \approx \int f(x)\phi_n(x)\,dx$$

where $\phi_n(x) = \phi(x-n)$. Substituting the above equation into (2) and differentiating it, we have

$$f'(x) = \sum_n f(n)\phi_n'(x). \tag{3}$$

Therefore, a function $f(x)$ can be approximated by (2), and its differential form $f'(x)$ can be approximated by (3). Based on these two approximations, we can represent all the function variables in (1) in a wavelet format. In this format, we have to calculate a number of integrals of products of several differential

TABLE I
TWO-TERM CONNECTION COEFFICIENTS: $\Gamma_i = \int \phi(x)\phi_i(x)\,dx$ AND $\Gamma'_i = \int \phi^{(x)}(x)\phi_i^{(x)}(x)\,dx$, OF DAUBECHIES' SCALING FUNCTION $\phi(x)$ WITH $N = 6$

i	Γ_i	Γ'_i
-4	0	-0.00535714285714
-3	0	-0.11428571428572
-2	0	0.87619047619047
-1	0	-3.39047619047619
0	1	5.26785714285715
1	0	-3.39047619047619
2	0	0.87619047619047
3	0	-0.11428571428572
4	0	-0.00535714285714

TABLE II
THREE-TERM CONNECTION COEFFICIENTS: $\Lambda_{i,j} = \int \phi(x)\phi_i(x)\phi_j(x)\,dx$, OF DAUBECHIES' SCALING FUNCTION $\phi(x)$ WITH $N = 6$

(i,j)	$\Lambda_{i,j}$	(i,j)	$\Lambda_{i,j}$	(i,j)	$\Lambda_{i,j}$
(4, 4)	-4.6492524e-06	(1, 4)	1.0186330e-06	(-2, 2)	-2.9257204e-06
(4, 3)	6.4355627e-06	(1, 3)	-5.6656771e-04	(-2, 1)	1.2067195e-03
(4, 2)	-2.9257204e-06	(1, 2)	-3.1707519e-02	(-2, 0)	2.3759883e-02
(4, 1)	1.0186330e-06	(1, 1)	9.0122957e-02	(-2, -1)	-3.1707519e-02
(4, 0)	1.2077707e-07	(1, 0)	1.5289039e-01	(-2, -2)	7.3133353e-03
		(1, -1)	-3.1707519e-02	(-2, -3)	-5.6656771e-04
		(1, -2)	1.2067195e-03	(-2, -4)	-2.9257204e-06
		(1, -3)	6.4355627e-06		
(3, 4)	6.4355627e-06	(0, 4)	1.2077707e-07	(-3, 1)	6.4355627e-06
(3, 3)	-8.5842521e-04	(0, 3)	2.1081922e-04	(-3, 0)	-8.5842521e-04
(3, 2)	1.2067195e-03	(0, 2)	7.3133353e-03	(-3, -1)	1.2067195e-03
(3, 1)	-5.6656771e-04	(0, 1)	1.5289039e-01	(-3, -2)	-5.6656771e-04
(3, 0)	2.1081922e-04	(0, 0)	9.4742170e-01	(-3, -3)	2.1081922e-04
(3, -1)	1.0186330e-06	(0, -1)	-9.0122957e-02	(-3, -4)	1.0186330e-06
		(0, -2)	2.3759883e-02		
		(0, -3)	-8.5842521e-04		
		(0, -4)	-4.6492524e-06		
(2, 4)	-2.9257204e-06	(-1, 3)	1.0186330e-06	(-4, 0)	-4.6492524e-06
(2, 3)	1.2067195e-03	(-1, 2)	-5.6656771e-04	(-4, -1)	6.4355627e-06
(2, 2)	2.3759883e-02	(-1, 1)	-3.1707519e-02	(-4, -2)	-2.9257204e-06
(2, 1)	-3.1707519e-02	(-1, 0)	-9.0122957e-02	(-4, -3)	1.0186330e-06
(2, -0)	7.3133353e-03	(-1, -1)	1.5289039e-01	(-4, -4)	1.2077707e-07
(2, -1)	-5.6656771e-04	(-1, -2)	-3.1707519e-02		
(2, -2)	-2.9257204e-06	(-1, -3)	1.2067195e-03		
		(-1, -4)	6.4355627e-06		

scaling functions with different orders, which are called connection coefficients and have been derived by Latto *et al.* [19].

The concept of connection coefficients is very useful for computing derivatives and solving differential equations. The general form of n-term connection coefficients is as follows [19]:

$$\Lambda_{l_2 \ldots l_n}^{d_1 d_2 \ldots d_n} = \int_{-\infty}^{\infty} \phi^{d_1}(x)\phi_{l_2}^{d_2}(x)\ldots\phi_{l_n}^{d_n}(x)\,dx$$

where $d_i \geq 0$ represents the differential order of the ith scaling function and l_i is the translation between $\phi^{d_1}(x)$ and $\phi^{d_i}(x)$. Once the derivative order $d_1, \ldots, d_n$ is determined, the function $\Lambda_{l_2 \ldots l_n}^{d_1 d_2 \ldots d_n}$ can be calculated for all combinations of $l_2, \ldots, l_n$. In [19], a technique was proposed for evaluating the two- and three-term connection coefficients. They define the scaling equations as homogeneous linear equations and the moment equations as inhomogeneous linear equations. These equations are used as bases to construct a linear system. Once the linear system is solved, the connection coefficients can be determined as well. For a specific problem, the connection coefficients of interest can be calculated in advance and then stored in tables for look-up use.

In this paper, we define a set of 1-D connection coefficients, which will be used in the computation of OF, as

$$\begin{aligned} \Gamma_i &= \int \phi(x)\phi_i(x)\,dx \\ \Gamma'_i &= \int \phi^{(x)}(x)\phi_i^{(x)}(x)\,dx \\ \Lambda_{i,j} &= \int \phi(x)\phi_i(x)\phi_j(x)\,dx \end{aligned} \qquad (4)$$

where $\phi^{(x)}(x) = (\partial/\partial x)\phi(x)$ and $\phi_i(x) = \phi(x - i)$. It is obvious that $\Gamma_0 = 1$ and $\Gamma_i = 0$, for all $i \neq 0$, due to the orthogonality property of the scaling function $\phi(x)$. Based on the technique described in [19], we can calculate the values of Γ_i, Γ'_i and $\Lambda_{i,j}$, which are illustrated in Tables I and II, respectively.

Fig. 1 shows the distribution of the function $\phi(x)$ with $N = 6$. Suppose the Daubechies scaling function is compactly supported in $[0, 1, \ldots, N-1]$ with its differentiability property; then, the significant domain of $\Lambda_{i,j}$ which has nonzero values is $2 - N \leq i, j \leq N - 2$, where $|i - j| \leq N - 2$. On the other hand, the significant domain of Γ'_i is $2 - N \leq i \leq N - 2$. In what follows, we will use wavelet-based approximation and connection coefficients to estimate the values of OF.

III. OF ESTIMATION

In this section, we will explain in detail how to apply wavelet approximation to model the OF problem. First of all, we reorganize (1) into the form

$$\begin{aligned} E = \iint \Big[\big(I_x^2 u^2 + I_y^2 v^2 + I_t^2 + 2I_x I_y uv + 2I_x I_t u \\ + 2I_y I_t v \big) + \alpha \left(u_x^2 + u_y^2 + v_x^2 + v_y^2 \right) \Big]\,dx\,dy. \end{aligned} \qquad (5)$$

Suppose the image size is $M \times M$. Based on the format defined in (2), the flow vector $[u(x,y), v(x,y)]$ can be represented as

$$\begin{aligned} u(x,y) &= \sum_{m=0}^{M-1} \sum_{n=0}^{M-1} u_{m,n}\phi(x-m, y-n) \\ v(x,y) &= \sum_{m=0}^{M-1} \sum_{n=0}^{M-1} v_{m,n}\phi(x-m, y-n) \end{aligned}$$

where $u_{m,n}$ and $v_{m,n}$ are the weighting coefficients, and the $\phi(x-m, y-n)$'s are the scaling bases of the subspace V_0 at the fine resolution 0. Once the weighting coefficients $u_{m,n}$

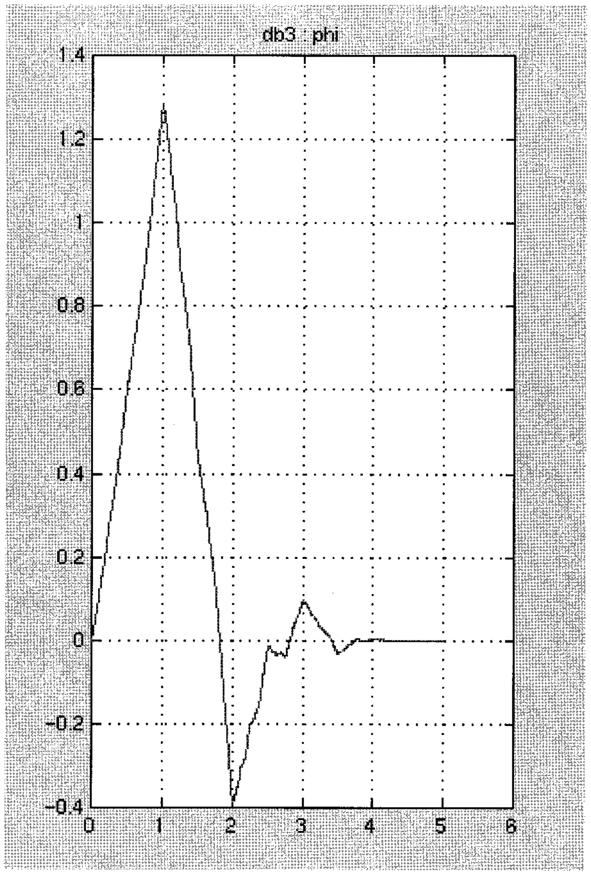

Fig. 1. Distribution of the Daubechies scaling function $\phi(x)$ with $N = 6$.

and $v_{m,n}$ of $u(x,y)$ and $v(x,y)$ are, respectively, determined, the OF problem can be solved. Therefore, we convert the OF problem into a process that involves determining the $2M^2$ nodal variables, $\{u_{m,n}\}$ and $\{v_{m,n}\}$, that will minimize the objective function E described in (5). Similarly, we apply wavelet approximation to represent image related functions as follows:

$$
\begin{aligned}
I_x^2(x,y) &= \sum_{m=0}^{M-1}\sum_{n=0}^{M-1} a_{m,n}\phi(x-m,y-n)\\
I_y^2(x,y) &= \sum_{m=0}^{M-1}\sum_{n=0}^{M-1} b_{m,n}\phi(x-m,y-n)\\
I_t^2(x,y) &= \sum_{m=0}^{M-1}\sum_{n=0}^{M-1} c_{m,n}\phi(x-m,y-n)\\
I_xI_y(x,y) &= \sum_{m=0}^{M-1}\sum_{n=0}^{M-1} d_{m,n}\phi(x-m,y-n)\\
I_xI_t(x,y) &= \sum_{m=0}^{M-1}\sum_{n=0}^{M-1} e_{m,n}\phi(x-m,y-n)\\
I_yI_t(x,y) &= \sum_{m=0}^{M-1}\sum_{n=0}^{M-1} f_{m,n}\phi(x-m,y-n).
\end{aligned}
$$

In order to avoid unbalanced weighting between the scales of flow vectors and those of image functions, the image functions are normalized by dividing $\sqrt{I_x^2 + I_y^2 + C}$, where C is a constant used to avoid dividing by zero. Throughout the experiments conducted in this study, C was constantly set to ten.

Plugging the above mentioned approximations of flow vector and image functions into (5) and reorganizing their formulations, we have

$$
\begin{aligned}
E = \iint \Bigg\{ & \left(\sum_{m,n} a_{m,n}\phi_{m,n}(x,y)\right)\left(\sum_{m,n} u_{m,n}\phi_{m,n}(x,y)\right)^2\\
&+ \left(\sum_{m,n} b_{m,n}\phi_{m,n}(x,y)\right)\left(\sum_{m,n} v_{m,n}\phi_{m,n}(x,y)\right)^2\\
&+ \left(\sum_{m,n} c_{m,n}\phi_{m,n}(x,y)\right) + 2\left(\sum_{m,n} d_{m,n}\phi_{m,n}(x,y)\right)\\
&\times \left(\sum_{m,n} u_{m,n}\phi_{m,n}(x,y)\right)\left(\sum_{m,n} v_{m,n}\phi_{m,n}(x,y)\right)\\
&+ 2\left(\sum_{m,n} e_{m,n}\phi_{m,n}(x,y)\right)\left(\sum_{m,n} u_{m,n}\phi_{m,n}(x,y)\right)\\
&+ 2\left(\sum_{m,n} f_{m,n}\phi_{m,n}(x,y)\right)\left(\sum_{m,n} v_{m,n}\phi_{m,n}(x,y)\right)\\
&+ \alpha\left[\left(\sum_{m,n} u_{m,n}\phi_{m,n}^{(x)}(x,y)\right)^2\right.\\
&\left. + \left(\sum_{m,n} u_{m,n}\phi_{m,n}^{(y)}(x,y)\right)^2\right]\\
&+ \alpha\left[\left(\sum_{m,n} v_{m,n}\phi_{m,n}^{(x)}(x,y)\right)^2\right.\\
&\left. + \left(\sum_{m,n} v_{m,n}\phi_{m,n}^{(y)}(x,y)\right)^2\right]\Bigg\}\, dx\, dy
\end{aligned}
\tag{6}
$$

where $\phi_{m,n}(x,y) = \phi(x-m, y-n), \phi_{m,n}^{(x)}(x,y) = (\partial/\partial x)\phi_{m,n}(x,y)$ and $\phi_{m,n}^{(y)}(x,y) = (\partial/\partial y)\phi_{m,n}(x,y)$. Here, the notation $\sum_{m,n}$ is the simplified form of $\sum_{m=0}^{M-1}\sum_{n=0}^{M-1}$. If we decompose the constraint function E in (6) as

$$
\begin{aligned}
E_1 &= \iint \left(\sum_{m,n} a_{m,n}\phi_{m,n}(x,y)\right)\\
&\quad \times \left(\sum_{m,n} u_{m,n}\phi_{m,n}(x,y)\right)^2 dx\, dy\\
E_2 &= \iint \left(\sum_{m,n} b_{m,n}\phi_{m,n}(x,y)\right)\\
&\quad \times \left(\sum_{m,n} v_{m,n}\phi_{m,n}(x,y)\right)^2 dx\, dy\\
E_3 &= \iint \left(\sum_{m,n} c_{m,n}\phi_{m,n}(x,y)\right) dx\, dy
\end{aligned}
$$

$$E_4 = \int\int \left(\sum_{m,n} d_{m,n}\phi_{m,n}(x,y)\right)\left(\sum_{m,n} u_{m,n}\phi_{m,n}(x,y)\right) \times \left(\sum_{m,n} v_{m,n}\phi_{m,n}(x,y)\right) dx\, dy$$

$$E_5 = \int\int \left(\sum_{m,n} e_{m,n}\phi_{m,n}(x,y)\right) \times \left(\sum_{m,n} u_{m,n}\phi_{m,n}(x,y)\right) dx\, dy$$

$$E_6 = \int\int \left(\sum_{m,n} f_{m,n}\phi_{m,n}(x,y)\right) \times \left(\sum_{m,n} v_{m,n}\phi_{m,n}(x,y)\right) dx\, dy$$

$$E_7 = \int\int \left(\sum_{m,n} u_{m,n}\phi^{(x)}_{m,n}(x,y)\right)^2 dx\, dy$$

$$E_8 = \int\int \left(\sum_{m,n} u_{m,n}\phi^{(y)}_{m,n}(x,y)\right)^2 dx\, dy$$

$$E_9 = \int\int \left(\sum_{m,n} v_{m,n}\phi^{(x)}_{m,n}(x,y)\right)^2 dx\, dy$$

and

$$E_{10} = \int\int \left(\sum_{m,n} v_{m,n}\phi^{(y)}_{m,n}(x,y)\right)^2 dx\, dy$$

then we have

$$E = \sum_{i=1}^{3} E_i + 2\sum_{i=4}^{6} E_i + \alpha\sum_{i=7}^{10} E_i.$$

Based on the basic properties learned from calculus and the definitions of connection coefficients, E_i can be easily derived which are shown in the Appendix.

According to the derivation results in Appendix, we can rewrite E as in (7), shown at the bottom of the page. Equation (7) is a quadratic and convex function of $\{u_{m,n}\}$ and $\{v_{m,n}\}$. From calculus of variations [20], we know that if one appropriately selects coordinate functions for variable approximation, then

$$\min_{\substack{u(x,y)\\ v(x,y)}} E(u(x,y), v(x,y)) = \min_{\substack{u_{m,n}\\ v_{m,n}}} E(u_{m,n}, v_{m,n}).$$

The optimal coefficients $\{\hat{u}_{m,n}, \hat{v}_{m,n}\}$ that will minimize $E(u_{m,n}, v_{m,n})$ can be determined by the stationary conditions

$$\frac{\partial E}{\partial \hat{u}_{m,n}} = 0 \quad \text{and} \quad \frac{\partial E}{\partial \hat{v}_{m,n}} = 0 \qquad \text{for } m,n = 0,\ldots,M-1.$$

The partial differential equations listed above form a large sparse linear system $\boldsymbol{Au} = \boldsymbol{b}$, where $\boldsymbol{u} = [\hat{u}_{0,0},\ldots,\hat{u}_{m,n},\ldots,\hat{u}_{M-1,M-1},\hat{v}_{0,0},\ldots,\hat{v}_{m,n},\ldots,\hat{v}_{M-1,M-1}]^t$ and the matrix $\boldsymbol{A} \in R^{2M^2\times 2M^2}$ is symmetric positive–definite with the following 2 × 2 block structure

$$\boldsymbol{A} = \begin{bmatrix} A_{11} & A_{12} \\ A_{21} & A_{22} \end{bmatrix}.$$

Here, $A_{12} = A_{21}$ and they are composed of $\sum_{i,j} d_{i,j}(\Lambda_{s-m,i-m}\Lambda_{t-n,j-n})$ with row index $m*M+n$ and column index $s*M+t$. Similarly, A_{11} is composed of $\sum_{i,j} a_{i,j}(\Lambda_{s-m,i-m}\Lambda_{t-n,j-n}) + \alpha(\Gamma'_{s-m}\Gamma_{t-n} + \Gamma_{s-m}\Gamma'_{t-n})$ and A_{22} has the same formula except $b_{i,j}$ is substituted for $a_{i,j}$. Since functions $\Lambda_{s-m,i-m}, \Gamma_{s-m}$, and Γ'_{t-n} are symmetric, any combination of two of them is also symmetric. Furthermore, the diagonals of A_{11} and A_{22} are all positive, thus the matrix A can be proved as positive definite. The well-structured large sparse linear system can be then solved without difficulty.

The wavelet-based method is superior to the traditional iterative methods due to the efficient and accurate approximation power of wavelets. With the traditional gradient-based methods, one often uses a pixel-wise iterative mechanism to solve the OF problem. At each iteration, each flow vector was computed independently and updated using local information that was computed in the previous iteration. On the other hand, our wavelet model collects information from flow field as well as image related functions concurrently and stores this information into the matrix $\boldsymbol{A}$. Once the linear system $\boldsymbol{Au} = \boldsymbol{b}$ is solved, the optimal coefficients $\{\hat{u}_{m,n}, \hat{v}_{m,n}\}$ can also be determined. Thus, we can successfully convert the problem of minimizing a constraint energy function, as depicted in (1), into that of solving a linear

$$\begin{aligned} E = &\sum_{m,n} u_{m,n} \sum_{s,t} u_{s,t}\left[\sum_{i,j} a_{i,j}(\Lambda_{s-m,i-m}\Lambda_{t-n,j-n})\right] + \sum_{m,n} v_{m,n}\sum_{s,t} v_{s,t}\left[\sum_{i,j} b_{i,j}(\Lambda_{s-m,i-m}\Lambda_{t-n,j-n})\right] + \sum_{m,n} c_{m,n} \\ &+ 2\sum_{m,n} u_{m,n}\sum_{s,t} v_{s,t}\left[\sum_{i,j} d_{i,j}(\Lambda_{s-m,i-m}\Lambda_{t-n,j-n})\right] \\ &+ 2\sum_{m,n} u_{m,n}\left[\sum_{i,j} e_{i,j}(\Gamma_{i-m}\Gamma_{j-n})\right] + 2\sum_{m,n} v_{m,n}\left[\sum_{i,j} f_{i,j}(\Gamma_{i-m}\Gamma_{j-n})\right] + \alpha\sum_{m,n} u_{m,n}\left[\sum_{s,t} u_{s,t}\left(\Gamma'_{s-m}\Gamma_{t-n}\right)\right] \\ &+ \alpha\sum_{m,n} u_{m,n}\left[\sum_{s,t} u_{s,t}\left(\Gamma_{s-m}\Gamma'_{t-n}\right)\right] + \alpha\sum_{m,n} v_{m,n}\left[\sum_{s,t} v_{s,t}\left(\Gamma'_{s-m}\Gamma_{t-n}\right)\right] + \alpha\sum_{m,n} v_{m,n}\left[\sum_{s,t} v_{s,t}\left(\Gamma_{s-m}\Gamma'_{t-n}\right)\right]. \end{aligned} \quad (7)$$

system of a convex and quadratic function. We then used the Incomplete Cholesky Preconditioned Conjugate Gradient method, provided in the SparseLib++ package, to solve this large linear system. Once the coefficients are determined, the flow vectors can be determined accordingly.

IV. Experimental Results

In our experiments, we used five sets of results obtained using five different methods for comparison. The five methods were those of Horn and Schunck [4], Barron *et al.* [1], Uras *et al.* [21], Anandan [22], and the proposed wavelet-based method. We used six standard image sequences to test the different methods.[1] The first three were image synthetic sequences, and the other three were real image sequences. The source codes included implementation of all the methods in [4], [1], [21], [22] and the error measurement. The angular error measurement between the correct velocity (u_c, v_c) and the estimated velocity (u_e, v_e) with 100% density is [1]

$$\theta_{\mathrm{err}} = \arccos\left(\frac{u_e u_c + v_e v_c + 1}{\sqrt{u_e^2 + v_e^2 + 1}\sqrt{u_c^2 + v_c^2 + 1}}\right).$$

The average errors and standard deviations of θ_{err} were calculated by neglecting a 20-pixel-wide boundary. The last image sequence was a standard test sequence in video compression. All experiments described in this section were pre-smoothed by a Gaussian filter with a sigma value of 1.5 and were sampled out to 3 standard deviation. The alpha value of the smoothness constraint was set to 0.2 for all the experiments conducted in this study. The number of iterations for Horn and Schunck's approach [4] and Barron *et al.*'s approach [1] were both set to 500. The parameters used in Uras *et al.*'s approach [21] and those in Anandan's approach [22] were set according to the experiments done in [1]. In our approach, computation of the flow fields was halted when the process for solving the linear system converged.

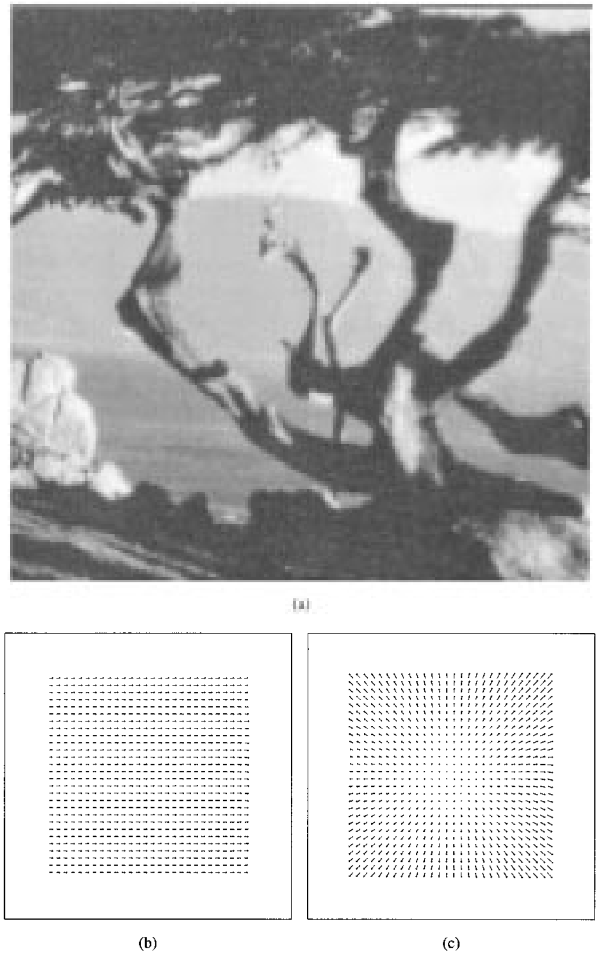

Fig. 2. Estimated OF for the Tree image sequences. (a) A frame grabbed from the synthetic Translating/Diverging Tree image sequences. (b) Estimated OF of the Translating Tree. (c) Estimated OF of the Diverging Tree.

TABLE III
COMPARISON RESULTS OBTAINED USING THE TRANSLATING TREE, THE DIVERGING TREE, AND YOSEMITE

	Translating Tree		Diverging Tree		Yosemite	
Method	Ave. Err	Std. Err	Ave. Err	Std. Err	Ave. Err	Std. Err
Horn and Schunck [4]	36.37°	27.60°	11.90°	11.10°	31.446°	30.188°
Barron et al. [1]	0.82°	0.92°	2.16°	2.16°	10.119°	15.651°
Uras et al. [21]	0.65°	0.64°	5.03°	3.69°	10.104°	15.533°
Anandan [22]	4.57°	3.04°	16.62°	12.39°	16.08°	14.421°
Our method	0.62°	0.66°	1.41°	1.23°	8.375°	13.395°

Figs. 2–7 show the experimental results obtained by applying Barron *et al.*'s method and our method. The estimated OFs shown in these figures were all subsampled and then rescaled. Fig. 2(a) shows one of the frames grabbed from the synthetic Translating/Diverging Tree image sequences; Fig. 2(b) and (c) shows the corresponding estimated OFs obtained using our proposed approach. The average errors and standard deviations of the computed flows for the above mentioned five methods are shown in Table III. The test images in the experiments were the 20th frame of the Translating Tree sequence and the 20th frame of the Diverging Tree sequence, respectively. Table III also shows the experimental results for Yosemite, where the test image was the ninth frame of the Yosemite sequence. From the results shown in Table III, it can be seen that our method outperformed the existing approaches. These results were not so obviously different because they were synthetic images. One thing to note is that we did not use the output data reported in the literature to make the comparison. This is because we changed some error-measurement criteria, such as the number of neglecting pixels in the boundary and the weighting of the smoothness constraint. In addition, we were not able to make the comparison with other wavelet-based approaches [12]–[14] because they did not release their source codes to the public. However, the readers can refer the experimental results reported in [12]–[14]. In what follows, we will present the results we obtained by applying our method to the real image sequences.

Fig. 3 shows two static frames grabbed from two standard real image sequences. Fig. 3(a) shows the ninth frame of the Hamburg Taxi image sequence. Fig. 3(b) shows a frame of an image sequence which had a rotating plate with a Rubik's cube on it. The difficulty in detecting the OF from the Rubik's image sequence was that the upper surface of the rotating plate was a very homogeneous region, so that only a little information could be used. Figs. 4 and 5 show the computed flow fields

[1] The first five image sequences and source codes implemented by Barron *et al.* [1] were taken from ftp.csd.uwo.ca.

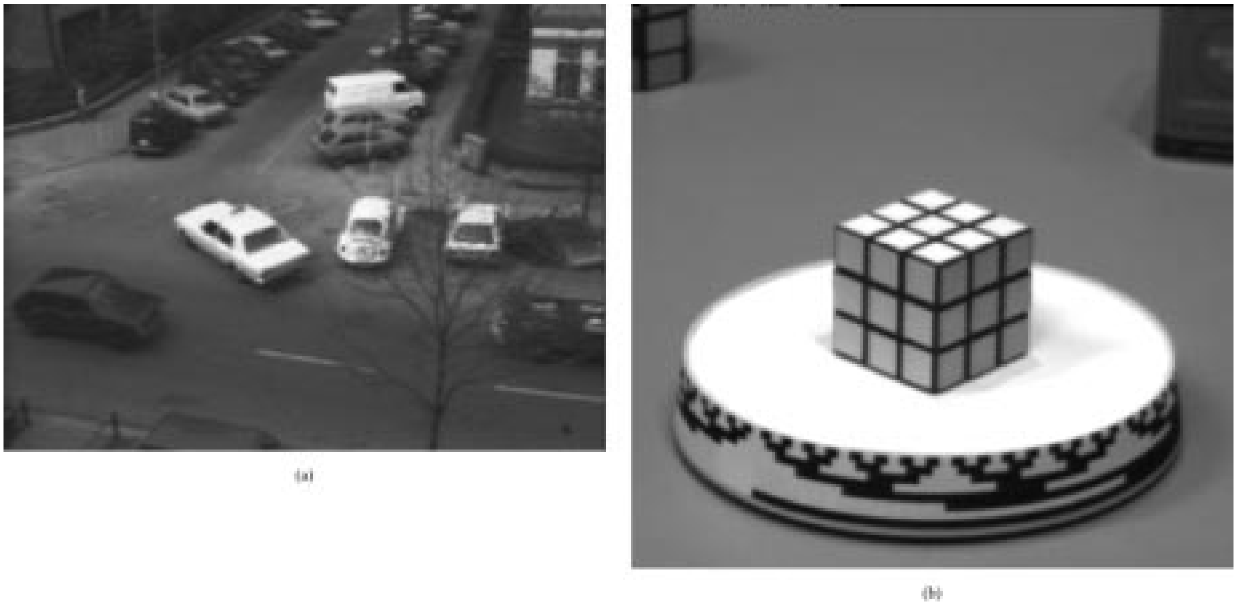

Fig. 3. Ninth frames, grabbed from the: (a) Hamburg Taxi and (b) rotating Rubik's image sequences.

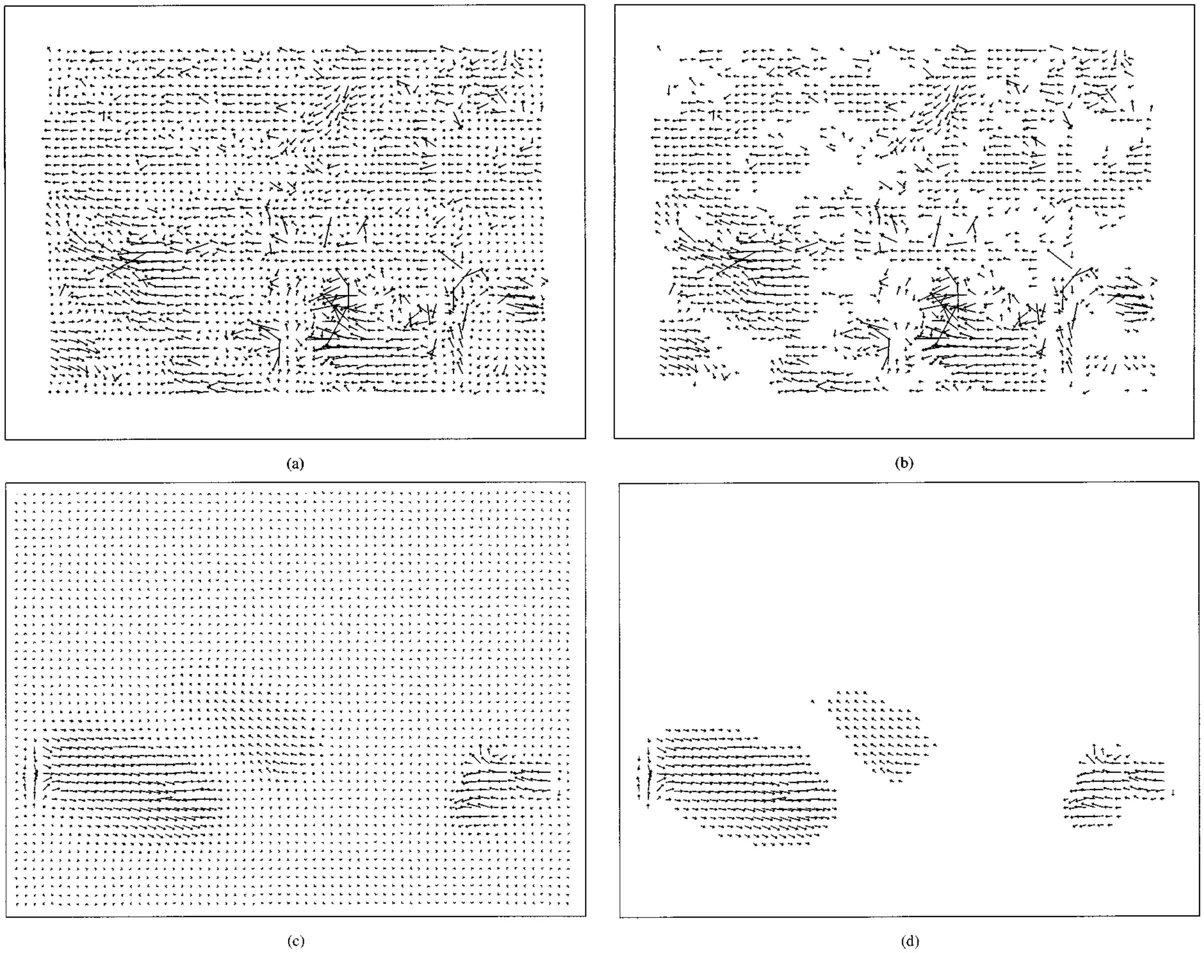

Fig. 4. Estimated OF from the Taxi image sequence obtained using Barron *et al.*'s approach. (a), (c) Obtained results (without setting a threshold) after 4:1 subsampling and 1:2 rescaling were performed. (b), (d) Obtained results from (a) and (c), respectively, by setting the threshold value to 0.8.

corresponding to Fig. 3(a) and (b), respectively. Fig. 4(a) and (c) show the results obtained (without setting a threshold) using Barron *et al.*'s [1] approach and our approach, respectively, after 4:1 subsampling and 1:2 rescaling. Fig. 4(b) and (d) show the results obtained from (a) and (c), respectively, by setting the threshold value to 0.8. From Fig. 4(d), we can see that three moving objects were located by our algorithm. Fig. 5(a) and (c) show the results obtained (without setting a threshold) using

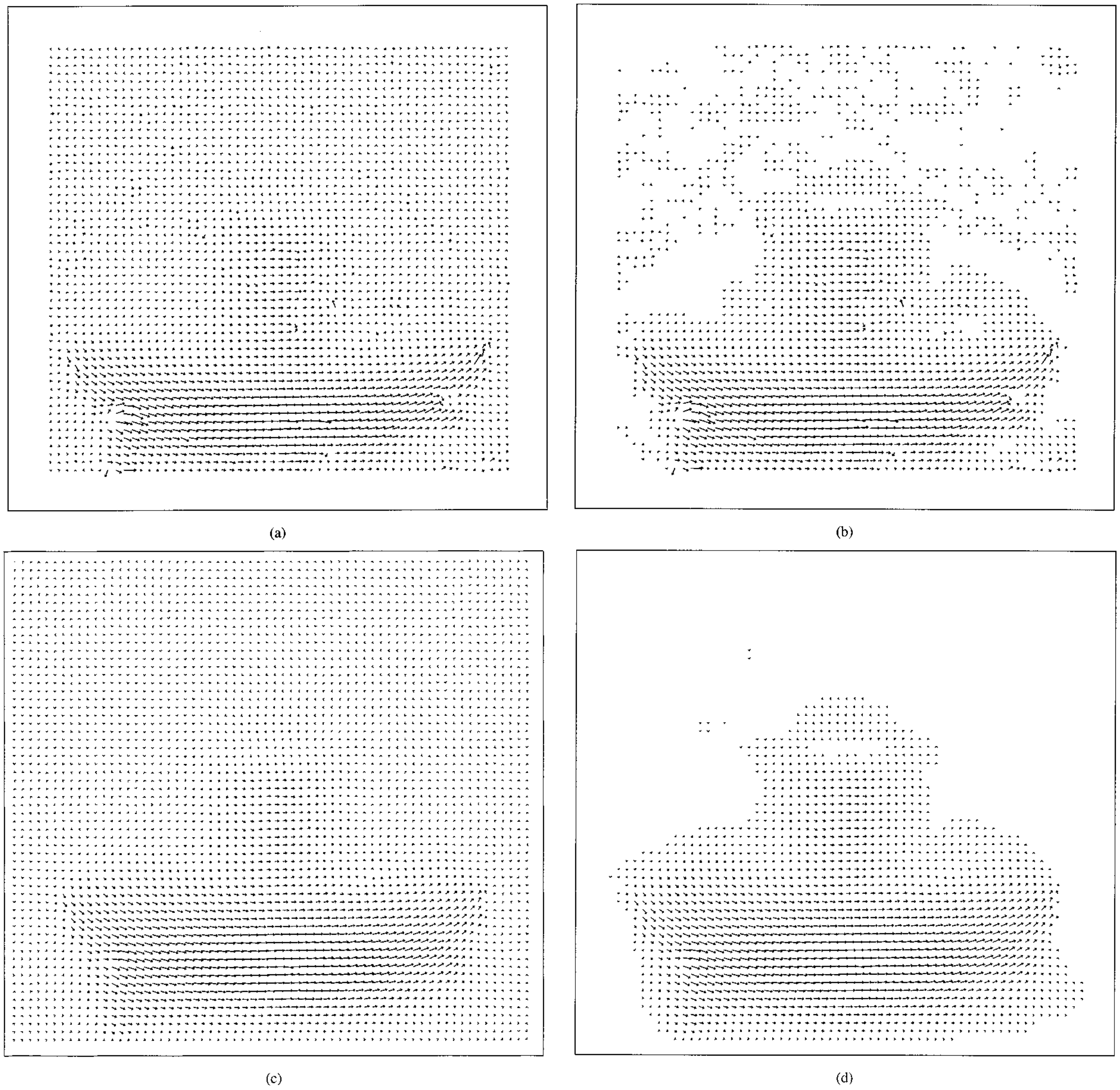

Fig. 5. Estimated OF obtained from the Rubik's image sequence using Barron *et al.*'s approach. (a), (c) Obtained results (without setting a threshold) after 4:1 subsampling and 1:3.5 rescaling were performed. (b), (d) Obtained results from (a) and (c), respectively, by setting the threshold value to 0.1.

Barron *et al.*'s [1] approach and our approach, respectively, after 4:1 subsampling and 1:3.5 rescaling. Fig. 5(b) and (d) show the thresholded results (with the threshold set to 0.1) for (a) and (c), respectively. From Fig. 5(d), it can be seen that the flow vectors of the rotating plate and the Rubik's cube were clearly captured by our algorithm. The result shown in Fig. 5(d) is very impressive. This is because the wavelet model has the ability to collect accurate information and to then spread it over the flow vector image. It is obvious that the flow vectors on the upper surface of the rotating plate, which was a homogeneous region, could be captured clearly and accurately.

Figs. 6 and 7 show a standard sequence in video compression: the Coastguard sequence. In acquiring this sequence, a video camera was fixated on a moving coastguard boat such that the boat was visually stationary. Fig. 6 was the 220th frame of the Coastguard sequence, and Figs. 7(a) and (c) show the results obtained (without setting a threshold) for Barron *et al.*'s approach and our proposed approach, respectively, after 3:1 subsampling and 1:1.5 rescaling. Fig. 7(b) and (d) show the thresholded results (with the threshold set to 0.3) for (a) and (c), respectively. Fig.7(d)

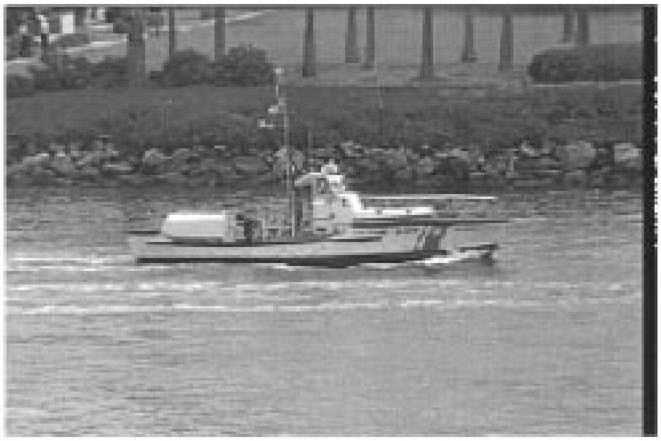

Fig. 6. 220th frame grabbed from the Coastguard sequence.

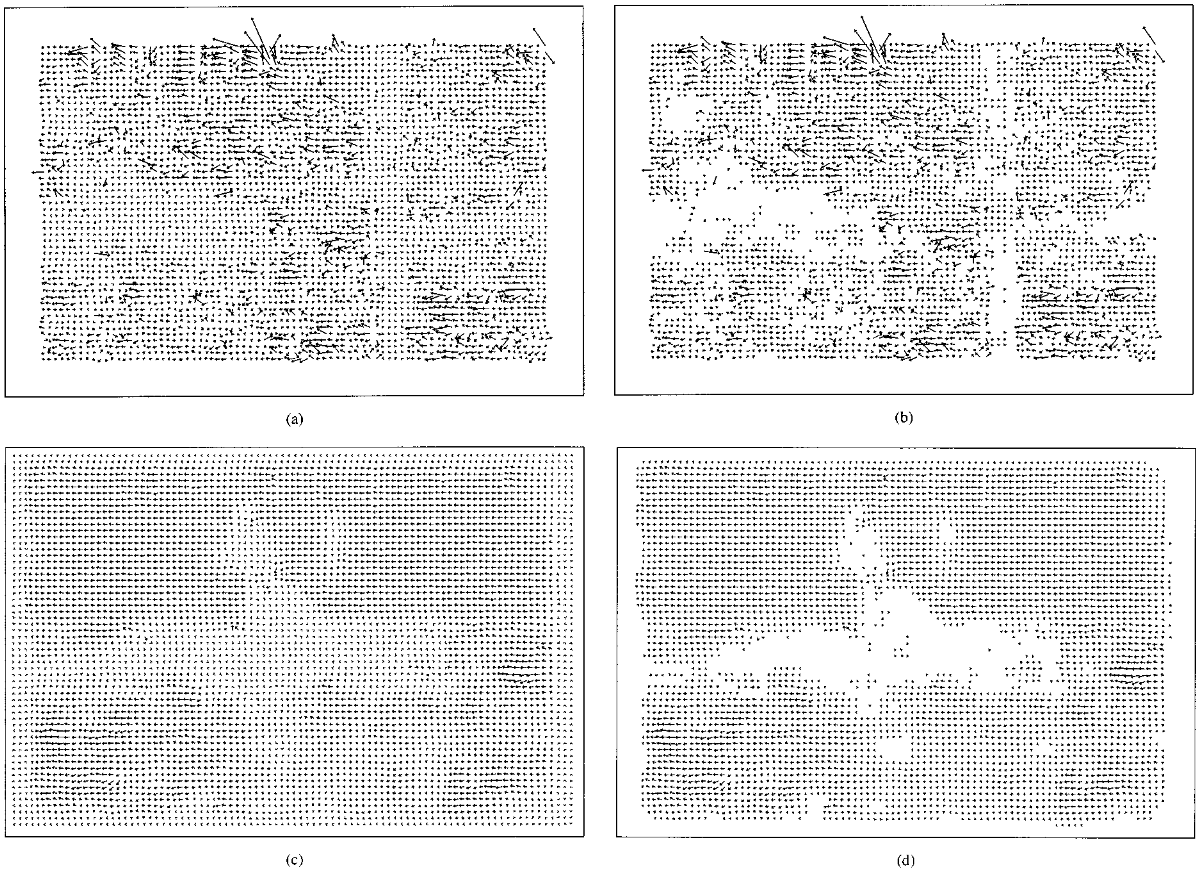

Fig. 7. (a) Estimated OF of the coastguard image sequence obtained using Barron *et al.*'s approach after 3:1 subsampling and 1:1.5 rescaling. (b) Result obtained from (a) by setting the threshold value to 0.3. (c) Estimated OF of the coastguard image sequence obtained using our proposed approach after 3:1 subsampling and 1:1.5 rescaling. (d) Result obtained from (c) by setting the threshold value to 0.3.

shows that the shape of the boat was nearly completely captured by our proposed method, even the tiny parts of the boat, such as the flag pole, the antenna, and the pole in front of the antenna.

As for the time complexity of the proposed method, two major parts were involved: 1) computation of the matrix $\boldsymbol{A}$ and 2) solving the large sparse linear system $\boldsymbol{Au} = \boldsymbol{b}$. Our method was implemented in C and all of our experiments were performed on a Sun Ultra 2 workstation with 512-MB RAM. The computational cost of the proposed method is proportional to the size of images. For divergence/translating tree sequences of size 150×150, it took about 30 s to compute the matrix $\boldsymbol{A}$ and another 80 s to solve the linear system. For the taxi sequence of size 190×256, it took about 75 s for computing $\boldsymbol{A}$ and about 320 s for solving the linear system. As for the rubic sequence of size 240×256, it took about 90 s for computation of the matrix $\boldsymbol{A}$ and 620 s for solving the linear system. These computations could be enhanced by applying preconditioners to sparse linear systems.

V. Discussion

In this paper, we called the proposed method "wavelet-based" because we adopted the translations of Daubechies' scaling functions as basis functions to perform wavelet transform in V_0 space. In traditional gradient-based approaches, they applied calculus of variations to iteratively estimate the flow field. In other wavelet-based methods, multiresolution property was utilized such that the flow estimation is done by interpolation of basis. However, all functions in our approach have been projected to V_0 space with finest resolution, such that we do not have to perform interpolation while doing reconstruction. The accuracy can be improved by estimating the flow field directly at the finest resolution without interpolation. Furthermore, applying wavelet transform to image functions can enhance system efficiency. This advantage can be revealed from the calculation of (7) in Section III. In the formulation, all scaling coefficients are unrelated to connection coefficients, and thus, they can be calculated in advance.

Another important property of wavelets is multiresolution. Applying multiresolution might speed up flow field estimation; however, some modifications will be necessary in our formulation. Such modifications will increase the complexity of our formulation and computational cost.

Regarding the computational complexity of the proposed method, the most time-consuming parts are the computation of the matrix $\boldsymbol{A}$ and solving the linear system $\boldsymbol{Au} = \boldsymbol{b}$. As for the construction of the matrix $\boldsymbol{A}$, because of its sparse and symmetric properties, only part of it need be computed. Regarding solving the linear system $\boldsymbol{Au} = \boldsymbol{b}$, the symmetric positive–definite property of the matrix $\boldsymbol{A}$ helps the convergence and efficiency of this linear system. The computation could also be enhanced by applying preconditioners to this sparse linear system. Such advantages make our method comparable to other wavelet-based methods in terms of computation complexity.

VI. Conclusion

In this paper, we have proposed a new algorithm for OF computation using a wavelet model. Based on wavelet transform, the original problem of minimizing the constraint function can be converted into that of solving a linear system of a quadratic and convex function of the scaling coefficients. Experimental results show that in terms of accuracy, our approach outperforms the existing methods which adopted the same objective function as ours. The results are quite convincing and encouraging especially in the homogeneous region, where the gradient-based methods usually hard to deal with. In fact, the proposed model can be applied to solve a great number of problems other than OF estimation, as long as they can be converted into the format for minimizing a quadratic energy function, for example, the gradient vector flow proposed in [23].

Appendix

E_1 can be written as

$$\begin{aligned} E_1 &= \sum_{m,n} u_{m,n} \sum_{s,t} u_{s,t} \left(\sum_{i,j} a_{i,j} \int\!\!\int \phi_{m,n}(x,y) \right. \\ &\qquad \left. \times\ \phi_{s,t}(x,y)\phi_{i,j}(x,y)\,dx\,dy \right) \\ &= \sum_{m,n} u_{m,n} \sum_{s,t} u_{s,t} \left(\sum_{i,j} a_{i,j} \int \phi_m(x)\phi_s(x) \right. \\ &\qquad \left. \times\ \phi_i(x)\,dx \int \phi_n(y)\phi_t(y)\phi_j(y)\,dy \right) \\ &= \sum_{m,n} u_{m,n} \sum_{s,t} u_{s,t} \left(\sum_{i,j} a_{i,j} \int \phi(x)\phi_{s-m}(x) \right. \\ &\qquad \left. \times\ \phi_{i-m}(x)\,dx \int \phi(y)\phi_{t-n}(y)\phi_{j-n}(y)\,dy \right) \\ &= \sum_{m,n} u_{m,n} \sum_{s,t} u_{s,t} \left(\sum_{i,j} a_{i,j}\Lambda_{s-m,i-m}\Lambda_{t-n,j-n} \right). \end{aligned}$$

The above equation is appropriate because 2-D connection coefficients can be converted into 1-D form based on the concept of the tensor product. These 1-D connection coefficients have been well defined in Section II. The same derivation can be applied to E_2 and E_4 to obtain

$$\begin{aligned} E_2 &= \sum_{m,n} v_{m,n} \sum_{s,t} v_{s,t} \left(\sum_{i,j} b_{i,j} \int\!\!\int \phi_{m,n}(x,y) \right. \\ &\qquad \left. \times\ \phi_{s,t}(x,y)\phi_{i,j}(x,y)\,dx\,dy \right) \\ &= \sum_{m,n} v_{m,n} \sum_{s,t} v_{s,t} \left(\sum_{i,j} b_{i,j}\Lambda_{s-m,i-m}\Lambda_{t-n,j-n} \right) \end{aligned}$$

and

$$\begin{aligned} E_4 &= \sum_{m,n} u_{m,n} \sum_{s,t} v_{s,t} \left(\sum_{i,j} d_{i,j} \int\!\!\int \phi_{m,n}(x,y) \right. \\ &\qquad \left. \times\ \phi_{s,t}(x,y)\phi_{i,j}(x,y)\,dx\,dy \right) \\ &= \sum_{m,n} u_{m,n} \sum_{s,t} v_{s,t} \left(\sum_{i,j} d_{i,j}\Lambda_{s-m,i-m}\Lambda_{t-n,j-n} \right). \end{aligned}$$

As for E_3, we can obtain

$$\begin{aligned} E_3 &= \sum_{m,n} c_{m,n} \int\!\!\int \phi_{m,n}(x,y)\,dx\,dy \\ &= \sum_{m,n} c_{m,n} \int \phi_m(x)\,dx \int \phi_n(y)\,dy \\ &= \sum_{m,n} c_{m,n} \end{aligned}$$

because $\int \phi_m(x)\,dx = \int \phi_n(y)\,dy = 1$.

For E_5 and E_6, we have

$$\begin{aligned} E_5 &= \sum_{m,n} u_{m,n} \left(\sum_{i,j} e_{i,j} \int\!\!\int \phi_{m,n}(x,y)\phi_{i,j}(x,y)\,dx\,dy \right) \\ &= \sum_{m,n} u_{m,n} \left(\sum_{i,j} e_{i,j} \int \phi_m(x)\phi_i(x)\,dx \right. \\ &\qquad \left. \times \int \phi_n(y)\phi_j(y)\,dy \right) \\ &= \sum_{m,n} u_{m,n} \left(\sum_{i,j} e_{i,j}\Gamma_{i-m}\Gamma_{j-n} \right) \end{aligned}$$

and

$$\begin{aligned} E_6 &= \sum_{m,n} v_{m,n} \left(\sum_{i,j} f_{i,j} \int\!\!\int \phi_{m,n}(x,y)\phi_{i,j}(x,y)\,dx\,dy \right) \\ &= \sum_{m,n} v_{m,n} \left(\sum_{i,j} f_{i,j}\Gamma_{i-m}\Gamma_{j-n} \right). \end{aligned}$$

Similarly, E_7 can be written as

$$\begin{aligned} E_7 &= \sum_{m,n} u_{m,n} \sum_{s,t} u_{s,t} \int\!\!\int \phi^{(x)}_{m,n}(x,y)\phi^{(x)}_{s,t}(x,y)\,dx\,dy \\ &= \sum_{m,n} u_{m,n} \sum_{s,t} u_{s,t} \int \phi^{(x)}_m(x)\phi^{(x)}_s(x)\,dx \\ &\qquad \times \int \phi_n(y)\phi_t(y)\,dy \\ &= \sum_{m,n} u_{m,n} \sum_{s,t} u_{s,t}\Gamma'_{s-m}\Gamma_{t-n}. \end{aligned}$$

The same derivation can be applied to E_8, E_9, and E_{10} to obtain

$$\begin{aligned}E_8 &= \sum_{m,n} u_{m,n} \sum_{s,t} u_{s,t} \int\int \phi^{(y)}_{m,n}(x,y)\phi^{(y)}_{s,t}(x,y)\,dx\,dy\\ &= \sum_{m,n} u_{m,n} \sum_{s,t} u_{s,t} \int \phi_m(x)\phi_s(x)\,dx\\ &\quad \times \int \phi^{(y)}_n(y)\phi^{(y)}_t(y)\,dy\\ &= \sum_{m,n} u_{m,n} \sum_{s,t} u_{s,t}\Gamma_{s-m}\Gamma'_{t-n}\\ E_9 &= \sum_{m,n} v_{m,n} \sum_{s,t} v_{s,t} \int\int \phi^{(x)}_{m,n}(x,y)\phi^{(x)}_{s,t}(x,y)\,dx\,dy\\ &= \sum_{m,n} v_{m,n} \sum_{s,t} v_{s,t}\Gamma'_{s-m}\Gamma_{t-n}\end{aligned}$$

and

$$\begin{aligned}E_{10} &= \sum_{m,n} v_{m,n} \sum_{s,t} v_{s,t} \int\int \phi^{(y)}_{m,n}(x,y)\phi^{(y)}_{s,t}(x,y)\,dx\,dy\\ &= \sum_{m,n} v_{m,n} \sum_{s,t} v_{s,t}\Gamma_{s-m}\Gamma'_{t-n}.\end{aligned}$$

Acknowledgment

The authors thank Dr. Yu-Te Wu of the Integrated Brain Research Unit, Department of Medical Research and Education, Taipei Veterans General Hospital, Taiwan, R.O.C., for the helpful discussion.

References

[1] J. L. Barron, D. J. Fleet, and S. S. Beauchemin, “Performance of optical flow techniques,” *Int. J. Comput. Vis.*, vol. 12, no. 1, pp. 43–77, 1994.

[2] S.-H. Lai and B. C. Vemuri, “Reliable and efficient computation of optical flow,” *Int. J. Comput. Vis.*, vol. 29, no. 2, pp. 87–105, 1998.

[3] E. P. Ong and M. Spann, “Robust optical flow computation based on least-median-of-squares regression,” *Int. J. Comput. Vis.*, vol. 31, no. 1, pp. 51–82, 1999.

[4] B. K. P. Horn and B. G. Schunck, “Determining optical flow,” *Artificial Intell.*, vol. 17, pp. 185–203, 1981.

[5] D. Terzopoulos, “Regularization of inverse visual problems involving discontinuities,” *IEEE Trans. Pattern Anal. Machine Intell.*, vol. PAMI-8, pp. 413–424, 1986.

[6] M. J. Black and P. Anandan, “The robust estimation of multiple motions: Parametric and piecewise-smooth flow fields,” *Comput. Vis. Image Understand.*, vol. 63, no. 1, pp. 75–104, 1996.

[7] J.-W. Hsieh, H.-Y. M. Laio, M.-T. Ko, and K.-C. Fan, “Wavelet-based shape from shading,” *Graph. Models Image Process.*, vol. 57, no. 4, pp. 343–362, 1995.

[8] G. Strang and T. Nguyen, *Wavelets and Filter Banks*. Cambridge, MA: Wellesley-Cambridge Press, 1996.

[9] S. Mallat, *A Wavelet Tour of Signal Processing*. New York: Academic, 1998.

[10] M. L. Resnikoff and R. O. Wells, *Wavelet Analysis: The Scalable Structure of Information*. New York: Springer-Verlag, 1998.

[11] T. J. Burns, S. K. Rogers, D. W. Ruck, and M. E. Oxley, “Discrete, spatiotemporal, wavelet multiresolution analysis method for computing optical flow,” *Opt. Eng.*, vol. 33, no. 7, pp. 2236–2247, 1994.

[12] C. P. Bernard, “Discrete wavelet analysis: A new framework for fast optic flow computation,” in *Proc. European Conf. Computer Vision*, Freiburg, Germany, June 1998, pp. 354–368.

[13] S. Srinivasan and R. Chellappa, “Optical flow using overlapped basis functions for solving global motion problems,” in *Proc. European Conf. Computer Vision*, Freiburg, Germany, June 1998, pp. 288–304.

[14] Y.-T. Wu, T. Kanade, J. Cohn, and C.-C. Li, “Optical flow estimation using wavelet motion model,” in *Proc. Int. Conf. Computer Vision*, Jan. 1998, pp. 992–998.

[15] ——, “Image registration using wavelet-based motion model,” *Int. J. Computer Vision*, vol. 38, no. 2, pp. 129–152, 2000.

[16] S. G. Mallat, “A theory for multiresolution signal decomposition: The wavelet representation,” *IEEE Trans. Pattern Anal. Machine Intell.*, vol. 11, pp. 674–693, 1989.

[17] R. O. Wells and X. Zhou, “Wavelet Interpolation and Approximate Solutions of Elliptic Partial Differential Equations,” Computat. Math. Lab., Rice Univ., Houston, TX, Tech. Rep., 1993.

[18] I. Daubechies, “Orthonormal bases of compactly supported wavelets,” *Commun. Pure Appl. Math.*, vol. 41, pp. 909–996, 1988.

[19] A. Latto, H. L. Resnikoff, and E. Tenenbaum, “The evaluation of connect coefficients of compactly supported wavelets,” in *Proc. USA-French Workshop on Wavelet and Turbulence*. NJ, 1991.

[20] F. Y. M. Wan, *Introduction to the Calculus of Variations and Its Applications*. London, U.K.: Chapman & Hall, 1995.

[21] S. Uras, F. Gorosi, A. Verri, and V. Torre, “A computational approach to motion perception,” *Biol. Cybernet.*, vol. 60, pp. 79–87, 1988.

[22] P. Anandan, “A computational framework and an algorithm for the measurement of visual motion,” *Int. J. Comput. Vis.*, vol. 2, pp. 283–310, 1989.

[23] C. Xu and J. L. Prince, “Snakes, shapes, and gradient vector flow,” *IEEE Trans. Image Processing*, vol. 7, pp. 359–369, Mar. 1998.

Li-Fen Chen (M’01) was born in Taiwan, R.O.C., in 1971. She received the B.S. and Ph.D. degrees in computer and information science from National Chiao Tung University, Taiwan, R.O.C., in 1993 and 2000, respectively.

She is currently a Postdoctoral Research Fellow in the Integrated Brain Research Unit, Department of Medical Research and Education, Taipei Veterans General Hospital, Taiwan, R.O.C. Her research interests include pattern recognition, image processing, computer vision, face recognition, medical image analysis, and wavelets. Her current research activities include exploring human brain functionalities using functional magnetic resonance imaging (fMRI), magneto-encephalo-graphy (MEG), and electro-encephalo-graphy (EEG).

Hong-Yuan Mark Liao (S’88–M’89–SM’01) received the B.S. degree in physics from National Tsing-Hua University, Hsin-Chu, Taiwan, in 1981, and the M.S. and Ph.D. degrees in electrical engineering from Northwestern University, Evanston, IL, in 1985 and 1990, respectively.

He was a Research Associate in the Computer Vision and Image Processing Laboratory, Northwestern University, during 1990–1991. In July 1991, he joined Institute of Information Science, Academia Sinica, Taiwan, R.O.C., as an Assistant Research Fellow. He was promoted to Associate Research Fellow and then Research Fellow in 1995 and 1998, respectively. From August 1997 to July 2000, he served as the Deputy Director of the institute. Currently, he is the Acting Director of Institute of Applied Science and Engineering Research, Academia Sinica. His research interests include multimedia signal processing, wavelet-based image analysis, content-based multimedia retrieval, and multimedia protection.

Dr. Liao served as the Program Chair of the International Symposium on Multimedia Information Processing (ISMIP’1997) and as Program Co-Chair of the 2nd IEEE Pacific-Rim Conference on Multimedia in 2001. He also served on the program committees of several international and local conferences. He is on the Editorial Boards of the IEEE Transactions on Multimedia, the *International Journal of Visual Communication and Image Representation*, the *Acta Automatica Sinica*, the *Tamkang Journal of Science and Engineering*, and the *Journal of Information Science and Engineering*. He was the recipient of the Young Investigators’ Award of Academia Sinica in 1998, the Excellent Paper Award in 1998 and 2000 and the Paper Award in 1996 and 1999, both from the Image Processing and Pattern Recognition Society of Taiwan.

Ja-Chen Lin was born in Taiwan, R.O.C. in 1955. He received the B.S. degree in computer science in 1977 and the M.S. degree in applied mathematics in 1979, both from National Chiao Tung University, Taiwan, R.O.C., and the Ph.D. degree in mathematics from Purdue University, West Lafayette, IN, in 1988.

From 1981 to 1982, he was an Instructor at National Chiao Tung University. From 1984 to 1988, he was a Graduate Instructor at Purdue University. He joined the Department of Computer and Information Science, National Chiao Tung University, in August 1988, and is currently a Professor there. His recent research interests include pattern recognition and image processing.

Dr. Lin is a member of the Phi-Tau-Phi Scholastic Honor Society.